Infinite Science
Publishing

Proceedings Article

Development of Optimized Magnetic Particle Imaging Tracers Utilizing Genetically Engineered Magnetosomes

Frank Mickoleit[c,*] · Florian Thieben[a,b] · Sophia Tessaro[c] · Peter Ludewig[a] · Dirk Schüler[c] · Javier Rández Garbayo[a] · René Uebe[c,d] · Tobias Knopp[a,b]

[a]University Medical Center Hamburg-Eppendorf, Hamburg, Germany
[b]Institute for Biomedical Imaging, Hamburg University of Technology, Hamburg, Germany
[c]Department of Microbiology, University of Bayreuth, Bayreuth, Germany
[d]Department of Microbial Biochemistry, University of Bayreuth, Bayreuth, Germany
*Corresponding author, email: Frank.Mickoleit@uni-bayreuth.de

Abstract

The imaging quality of Magnetic Particle Imaging (MPI) is not just limited by the MPI system but also by the quality of available tracers. The tracer quality can be improved by optimizing the shape, core size and shell of the nanoparticles. However, such a defined synthesis is quite challenging. Biogenic magnetic nanoparticles, so-called magnetosomes, synthesized by magnetotoactic bacteria, might provide a promising alternative. In this study, magnetosomes isolated from different *Magnetospirillum gryphiswaldense* mutant strains biomineralizing particles with varying core diameters were investigated with regard to their usability as tracers for MPI.

I. Introduction

Magnetic Particle Imaging (MPI) is a new radiation-free tomographic imaging method with superior temporal resolution compared to other conventional imaging methods [1]. As a tracer-based imaging modality, the imaging process of MPI relies on the nonlinear magnetization response of the tracer materials to time varying magnetic fields. Therefore, imaging performance critically depends on the physical parameters of the tracer particles like, for example, the material and structure of the crystal but also its shape and size [2]. In theory, a magnetic core diameter of approx. 25 to 28 nm with a high magnetic moment within a single magnetic domain particle is desirable [2]. However, the abiotic synthesis of such optimized particles depends on a wide range of parameters and is therefore quite chal-

lenging. A promising alternative tracer "material" are magnetosomes [3, 4], biogenic magnetic nanoparticles biosynthesized by magnetotactic bacteria (MTB). In the model MTB *Magnetospirillum gryphiswaldense*, magnetosomes consist of a cuboctahedral magnetite core that is surrounded by a biological membrane of phospholipids and a set of >30 magnetosome-specific proteins [5]. These proteins fulfill essential functions in magnetite biomineralization [6] and thereby enable the controlled synthesis of particles of 35 to 40 nm in diameter that are characterized by a high crystallinity, strong magnetization and a narrow particle size distribution (Gaussian to logarithmic-normal size distribution [3]) that can only hardly be achieved by chemical synthesis. Even more interestingly, modification of magnetosome-related genes by synthetic biology approaches enables the biosynthesis of size-adjusted magnetite crystals [6] with different

magnetic properties [7, 8].

In this work, we investigated different (engineered) magnetosomes as improved imaging agents for MPI. For this purpose, we isolated particles from the wildtype (WT) as well as seven different *M. gryphiswaldense* deletion strains with core diameters in the size range from 20 to 40 nm. After analyzing the size distribution by transmission electron microscopy (TEM), we used magnetic particle spectroscopy (MPS) to identify particle "candidates" with promising 1D-signal responses compared to the standard tracer perimag. Our results show that certain mutant magnetosomes of types $\Delta feoAB1$, $\Delta feoAB12$ and $\Delta Fe4$ resulted in significantly improved MPS signals, and therefore, enhanced MPI signals.

II. Methods and materials

Bacterial strains and cultivation conditions. For the production of size-adjusted magnetosome samples, genetically modified *M. gryphiswaldense* strains $\Delta mamR$, $\Delta mamF$, $\Delta mamF/mmsF$ (each from [6]), $\Delta mamJ$ [9], and $\Delta feoAB1$ [8] were used. Additionally, we generated a *feoAB12* double mutant by deletion of the *feoAB2* genes within the $\Delta feoAB1$ strain using a previously published *galK*-based counterselection method [10].

Bacterial strains (*M. gryphiswaldense* WT and mutants) were grown in modified flask standard medium (FSM) as previously described [11]. Cultivation was performed in 5 L flasks under moderate shaking (120 rpm) at 28 °C, applying a headspace-to-liquid ratio of 1:4 with air in the headspace. Under these conditions, the oxygen concentration in the medium declined with increasing cell density, thereby reaching microoxic conditions and inducing magnetosome biosynthesis. Cells were harvested in the late exponential growth phase by centrifugation (9000 g, 20 min, 4 °C), and stored at −20 °C until further use.

Magnetosome isolation. For the isolation of intact magnetosomes, a two-step purification procedure consisting of a magnetic separation and a sucrose high-density ultracentrifugation step was applied [11]. To further remove microbial contaminations, magnetosome suspensions were sterile-filtrated as previously described [12] and adjusted to a final Fe concentrations of 2 mg/mL (35.7 mmol/L).

Transmission electron microscopy. For TEM analyses, the respective samples (highly diluted magnetosome suspensions) were directly deposited onto carbon-coated copper grids (Science Services, Munich, Germany). TEM was performed on a JEM-1400Plus transmission electron microscope (JEOL, Tokyo, Japan) operated with an acceleration voltage of 80 kV and the magnetosome core sizes were measured.

Determination of iron concentrations. Suspensions of isolated magnetosomes were normalized to their over-
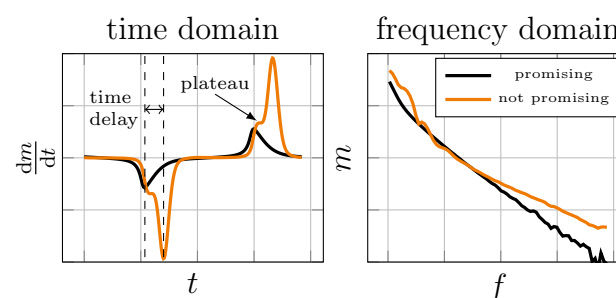
Figure 1: Acquired example data of a promising and a non-promising MPS signal response. The promising signal response shows a single amplitude in time domain (left) and a smooth signal decay in frequency domain (right). A non-promising signal response can be identified in time domain by a time delayed amplitude or a plateau. In frequency domain this results in a not smooth frequency decay.

all iron concentration. The iron content (mg_{Fe}/mL) was determined by atomic absorption spectroscopy (AAS) as previously described [11] using a contrAA300 high-resolution atomic absorption spectrometer (Analytik Jena, Jena, Germany).
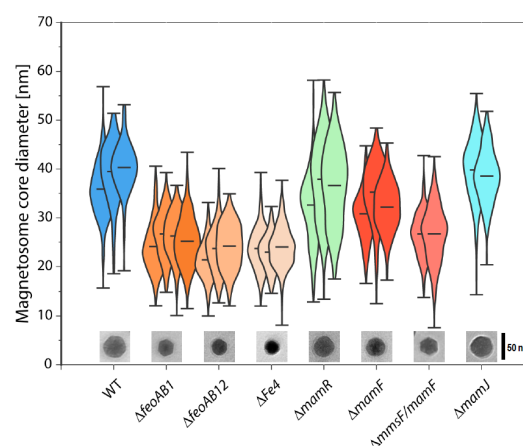
Figure 2: Violin plot of the core size distribution of magnetosomes isolated from different *M. gryphiswaldense* strains as indicated. Each particle suspension was analyzed by TEM, and ImageJ software was used to determine the core diameters ($n \geq 350$). The insets show TEM micrographs of a representative magnetosome particle isolated from the respective strain.

Magnetic particle spectroscopy. The MPI performance of the synthesized magnetosomes was studied by MPS measurements. From each batch a 10 μL-sample containing 2 mg_{Fe}/mL was measured. For reference, a 10 μL-sample of pre-clinical MPI tracer perimag (micromod Partikeltechnologie, Rostock, Germany) (∼19 nm core diameter) containing the same iron concentration was used. Utilizing a calibrated custom MPS [13], the samples were excited with a 20 mT/μ_0 drive field at 26.042 kHz.
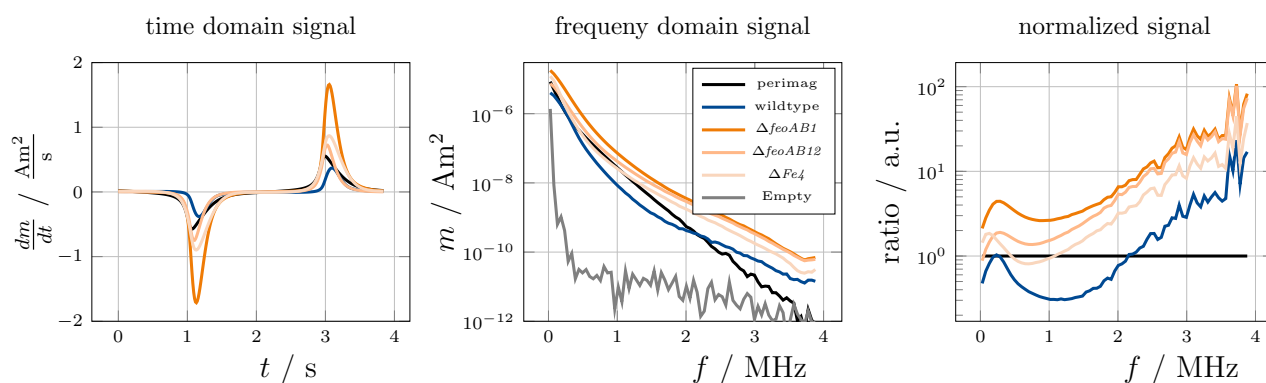
Figure 3: MPS measurements of promising magnetosome strains. The time domain signals are shown on the left. In the middle, the corresponding frequency domain signals, together with an empty measurement are shown. The frequency signals normalized to perimag are depicted on the right.

The MPS signal responses were evaluated in time domain, frequency domain and normalized to the reference signal response of perimag. The assessment of the MPS signal responses was carried out visually, taking into account three factors: First, a similar or better MPS signal response compared to perimag. In time domain the amplitude of the signal responses can be compared and in the frequency domain, the signal decay can additionally be considered. Here, a slow signal decay is beneficial. Second, a single amplitude in time domain without a plateau. A time-delayed amplitude with a stronger second peak can be attributed to agglomeration, where a certain energy potential is required to change the magnetization. At lower drive-field amplitudes this higher and time-delayed amplitude disappears. The third and last factor is a smooth signal decay in frequency domain. To illustrate this behavior, in Figure 1 a measured example of a promising and a non-promising MPS signal response is shown.

III. Results

Physicochemical characterization. In Figure 2 the iron-core size distribution for all isolated magnetosome samples is shown. Magnetosomes of the mutant strains $\Delta mamR$, $\Delta mamJ$, and $\Delta mamF$ showed similar or slightly smaller diameters compared to the WT and are thus above the threshold size for superparamagnetism for cubic magnetite particles [14]. In contrast, the mean core diameter of the $\Delta feoAB1$, $\Delta feoAB12$, $\Delta Fe4$, and $\Delta mmsF/mamF$ magnetosome samples were significantly smaller than the WT and ranged in the superparamagnetic domain size range between 21 to 28 nm. While there is a weak trend towards lower standard deviations for samples with small magnetosome core diameters, all magnetosome types show a rather wide size distribution. Furthermore, on TEM micrographs for magnetosome samples being in the ferrimagnetic size range, increased

tendencies to form chains, rings or aggregates were observed, whereas particles in the superparamagnetic size range appeared to be rather well-dispersed (data not shown).

Magnetic particle spectroscopy. Figure 3 shows examples of promising magnetosome samples from strains $\Delta feoAB1$, $\Delta feoAB12$, $\Delta Fe4$ and the WT. These signal responses show a single amplitude in time domain, a smooth signal decay in frequency domain and beside the WT, they all exceed the MPS signal response of perimag. In contrast, magnetosome samples of the $\Delta mamR$, $\Delta mamJ$, $\Delta mmsF/mamF$ and $\Delta mamF$ strains did not show the desired signal response and were subsequently not considered further (data not shown).

IV. Discussion and conclusion

Here, we demonstrate that MPS is a reliable tool to exclude unsuitable magnetosomes by examining their magnetization signal response. Although the magnetic isolation procedure narrows the particle size distribution [11], the particles are still polydisperse, which is based on the biological synthesis since the particles are synthesized gradually and become larger during maturation. Using MPS measurements we could identify promising magnetosome types. Thereby, the MPS signal response increased for $\Delta Fe4$, $\Delta feoAB12$ and $\Delta feoAB1$ magnetosomes with their increasing core diameter. In conclusion, the synthesis of superparamagnetic magnetosomes seems to be highly promising for optimized MPI tracers. According to [2], the mean iron-core diameter of magnetosomes from strains $\Delta feoAB1$, $\Delta feoAB12$, $\Delta Fe4$ and $\Delta mmsF/mamF$ is in the range of optimal MPI tracers. $\Delta feoAB1$ magnetosomes were identified as perfect candidates for further MPI experiments, since their time-domain amplitude is a factor of 2.99 higher compared to perimag.

Acknowledgments

Author's statement

Conflict of interest: Authors state no conflict of interest.

References

[1] P. Ludewig, M. Graeser, N. D. Forkert, F. Thieben, J. Rández-Garbayo, J. Rieckhoff, K. Lessmann, F. Förger, P. Szwargulski, T. Magnus, *et al.* Magnetic particle imaging for assessment of cerebral perfusion and ischemia. *Wiley Interdisciplinary Reviews: Nanomedicine and Nanobiotechnology*, 14(1):e1757, 2022.

[2] C. Shasha, E. Teeman, and K. M. Krishnan. Nanoparticle core size optimization for magnetic particle imaging. *Biomedical Physics & Engineering Express*, 5(5):055010, 2019.

[3] A. Kraupner, D. Eberbeck, D. Heinke, R. Uebe, D. Schüler, and A. Briel. Bacterial magnetosomes–nature's powerful contribution to mpi tracer research. *Nanoscale*, 9(18):5788–5793, 2017.

[4] A. V. Makela, M. A. Schott, C. S. Madsen, E. M. Greeson, and C. H. Contag. Magnetic particle imaging of magnetotactic bacteria as living contrast agents is improved by altering magnetosome arrangement. *Nano Letters*, 22(12):4630–4639, 2022, PMID: 35686930. doi:10.1021/acs.nanolett.1c05042.

[5] R. Uebe and D. Schüler. Magnetosome biogenesis in magnetotactic bacteria. *Nature Reviews Microbiology*, 14:621–637, 2016, doi:10.1038/nrmicro.2016.99.

[6] A. Lohße, S. Borg, O. Raschdorf, I. Kolinko, É. Tompa, M. Pósfai, D. Faivre, J. Baumgartner, and D. Schüler. Genetic dissection of the mamab and mms6 operons reveals a gene set essential for magnetosome biogenesis in magnetospirillum gryphiswaldense. *Journal of bacteriology*, 196(14):2658–2669, 2014.

[7] R. Taukulis, M. Widdrat, M. Kumari, D. Heinke, M. Rumpler, É. Tompa, R. Uebe, A. Kraupner, A. Cebers, D. Schüler, *et al.* Magnetic iron oxide nanoparticles as mri contrast agents-a comprehensive physical and theoretical study. *Magnetohydrodynamics*, 51(4):721–747, 2015.

[8] D. Heinke, A. Kraupner, D. Eberbeck, D. Schmidt, P. Radon, R. Uebe, D. Schüler, and A. Briel. Mps and mri efficacy of magnetosomes from wild-type and mutant bacterial strains. *International Journal on Magnetic Particle Imaging*, 3(2), 2017.

[9] A. Scheffel, M. Gruska, D. Faivre, A. Linaroudis, J. M. Plitzko, and D. Schüler. An acidic protein aligns magnetosomes along a filamentous structure in magnetotactic bacteria. *Nature*, 440(7080):110–114, 2006.

[10] O. Raschdorf, J. M. Plitzko, D. Schüler, and F. D. Müller. A tailored galk counterselection system for efficient markerless gene deletion and chromosomal tagging in magnetospirillum gryphiswaldense. *Applied and environmental microbiology*, 80(14):4323–4330, 2014.

[11] S. Rosenfeldt, F. Mickoleit, C. Jörke, J. H. Clement, S. Markert, V. Jérôme, S. Schwarzinger, R. Freitag, D. Schüler, R. Uebe, *et al.* Towards standardized purification of bacterial magnetic nanoparticles for future in vivo applications. *Acta Biomaterialia*, 120:293–303, 2021.

[12] F. Mickoleit, V. Jérôme, R. Freitag, and D. Schüler. Bacterial magnetosomes as novel platform for the presentation of immunostimulatory, membrane-bound ligands in cellular biotechnology. *Advanced Biosystems*, 4(3):1900231, 2020.

[13] F. Thieben, T. Knopp, M. Boberg, F. Foerger, M. Graeser, and M. Möddel. On the receive path calibration of magnetic particle imaging systems. *IEEE Transactions on Instrumentation and Measurement*, 72:1–15, 2023, doi:10.1109/TIM.2022.3219461.

[14] A. R. Muxworthy and W. Williams. Critical superparamagnetic/single-domain grain sizes in interacting magnetite particles: Implications for magnetosome crystals. *Journal of the Royal Society Interface*, 6(41):1207–1212, 2009.